BAREKENG: Journal of Mathematics and Its Applications
December 2026 Volume 20 Issue 4 Page 3067-3082
P-ISSN: 1978-7227 E-ISSN: 2615-3017
https://doi.org/10.30598/barekengvol20iss4pp3067-3082

# A NUMERIC STUDY OF MATERIAL DISPERSION CONTROL IN A RESERVOIR FROM THREE POINTS BASES

**Nurcahya Yulian Ashar** [1], **Muhammad Manaqib** [2*], **Yoga Amanda Putra** [3]

[1]*Department of Mathematics, Faculty of Sciences and Mathematics, Universitas Diponegoro*
*Jln. Prof Jacob Rais, Tembalang, Kota Semarang, 50275, Indonesia*

[2,3]*Department of Mathematics, Faculty of Science and Technology,*
*Universitas Islam Negeri Syarif Hidayatullah Jakarta*
*Jln. Ir. H. Juanda No. 95, Ciputat, Kec. Ciputat, South Tangerang, 15412, Indonesia*

*Corresponding author's e-mail: * **muhammad.manaqib@uinjkt.ac.id***

**Article Info**

***Article History:***

*Received: 27th September 2025*
*Revised: 2nd April 2026*
*Accepted: 28th May 2026*
*Available online: 1st July 2026*

***Keywords:***

*Convection-Diffusion;*
*Differential Equation;*
*DRBEM;*
*Mathematical Model.*

**ABSTRACT**

*This study aims to optimize material dispersion in a reservoir with turbulent flow using the convection-diffusion equation with three-point sources, addressing a research gap from previous studies that utilized only two sources. The Dual Reciprocity Boundary Element Method (DRBEM) is applied as a numerical solution, with flow characteristics simulated using the k-epsilon turbulence model. Ten configurations of source point positions were evaluated to determine the most effective strategy for uniform material distribution. Results demonstrate that DRBEM accurately approximates analytical solutions, with improved accuracy at higher interpolation point densities. The key finding reveals that Case 2 (vertical arrangement at the downstream side) yields the most uniform distribution, achieving ~8.53% higher uniformity compared to other cases. While limited to a specific velocity profile and boundary conditions, this research provides valuable insights for engineering applications in reservoir management by identifying optimal source placement strategies.*



***How to cite this article:***

N. Y. Ashar, M. Manaqib, and Y. A. Putra, "A NUMERIC STUDY OF MATERIAL DISPERSION CONTROL IN A RESERVOIR FROM THREE POINTS BASES", *BAREKENG: J. Math. & App.*, vol. 20, no. 4, pp. 3067-3082, Dec. 2026.


Journal homepage: *https://ojs3.unpatti.ac.id/index.php/barekeng/*
Journal e-mail: *barekeng.math@yahoo.com; barekeng.journal@mail.unpatti.ac.id*

**Research Article · Open Access**

## 1. INTRODUCTION

Quantitative modeling is one of the crucial topics in the field of applied mathematics and physics. Through modeling, various natural phenomena can be understood more deeply and systematically. In general, the aim of mathematical modeling is to study a problem efficiently, including efforts to minimize research costs. One interesting equation of modeling to explore is the convection-diffusion equation, particularly because of its wide applications in various physical and mathematical problems. The distribution of material in a reservoir will be examined using a convection-diffusion equation approach. Before applying the model to the problem, it is essential to address the process of its quantitative derivation. In the previous research, Samec et al. [1] and Stynes [2] obtained the convection-diffusion equation in a mathematical framework capable of addressing the issue of material dispersion within certain boundaries or domains. Next, analytical solutions of the diffusion-convection equation were derived by Morales-Delgado et al. [3] and also Polyanin [4]. Analytical solutions are generally limited to specific Cases, particularly those with simpler configurations. For more complex scenarios, such as the dispersion of materials in a reservoir, numeric approaches are required. This paper presents a numerical study of the material dispersion problem within the reservoir domain.

Numeric methods are one of the possible approaches to solving the convection-diffusion equation with source points. Several researchers have conducted studies to solve the convection-diffusion equation. The convection-diffusion equation was addressed by Zhang et al. [5], Wang et al. [6], and He et al. [7] without the inclusion of source points in the governing equations. In contrast, Ashar and Hariyanto [8] have studied the convection-diffusion equation with two source points, which we find a research gap for source points more than two. This research will examine the convection-diffusion equation with three source points, continuing the study conducted by Ashar and Hariyanto [8].

The convection-diffusion equation with source points is particularly suitable for solving using the DRBEM [9]. DRBEM is an expansion of the Boundary Element Method (BEM), which is one of the numerical methods for solving differential equations. DRBEM has proven successful in numerically solving several partial differential equation problems. For example, Manaqib [10] studied the solution of furrow irrigation infiltration problems on various types of homogeneous soil. Other researchers who have studied infiltration in irrigation channels include Clement and Lobo [11], Solekhudin and Ang [12], Solekhudin [13], Munadi et al. [14], Ashar [15], and Ashar and Solekhudin [16]. Recent research related to this method is explained by Alsoy-Akgün [17], Zahroh et al. [18], and Priya et al. [19]. In these studies, DRBEM demonstrated its flexibility in solving different types of problems with various simple closed domain shapes. In this paper, DRBEM will be utilized to resolve the problem of material dispersion in a reservoir with three-point bases. Several combinations of source point locations will be shown to determine which point location is most effective in material distribution.

## 2. RESEARCH METHODS

In this part, the mathematical derivation of the convection-diffusion equation is presented, along with the derivation of DRBEM employed to solve the problem. The mathematical model of the convection-diffusion equation considered in this study is given by Eq. (1), defined on a domain $R$ bounded by a simple closed curve $C$.

$$\frac{\partial U(x,y)}{\partial x} w_1(x,y) + \frac{\partial U(x,y)}{\partial y} w_2(x,y) - D\left(\frac{\partial^2 U(x,y)}{\partial x^2} + \frac{\partial^2 U(x,y)}{\partial y^2}\right) = G(x,y), \tag{1}$$

where $U$ is the concentration of material, $w_1(x,y)$ and $w_2(x,y)$ are liquid velocity within $x$ and $y$ directions, $D$ is the diffusion coefficient of the material in the liquid, and $G$ is a function of source points. The problem with source points is defined by Eq. (2).

$$\frac{\partial U(x,y)}{\partial x} w_1(x,y) + \frac{\partial U(x,y)}{\partial y} w_2(x,y) - D\left(\frac{\partial^2 U}{\partial x^2} + \frac{\partial^2 U}{\partial y^2}\right) = G(x,y)\sigma(x,y;a,b), \tag{2}$$

where $(a,b)$ denotes the coordinates of the source point, and $\sigma(x,y;a,b)$ is a Dirac delta function with source points $(a,b)$. DRBEM is applying to solve the Eqs. (1) and (2) numerically, by transforming the governing equation into its corresponding boundary integral equation, as given below.

$$\lambda(\xi,\eta)U(\xi,\eta)=\int_C\left[U(x,y)\frac{\Phi(x,y;\xi,\eta)}{\partial n}-\Phi(x,y;\xi,\eta)\frac{U(x,y)}{\partial n}\right]ds$$
$$+\frac{1}{D}\iint_R\Phi(x,y;\xi,\eta)\left[w_1(x,y)\frac{U(x,y)}{\partial x}+w_2(x,y)\frac{U(x,y)}{\partial y}-G(x,y)\right]dxdy \quad (3)$$

and

$$\lambda(\xi,\eta)U(\xi,\eta)=\int_C\left[U(x,y)\frac{\Phi(x,y;\xi,\eta)}{\partial n}-\Phi(x,y;\xi,\eta)\frac{U(x,y)}{\partial n}\right]ds$$
$$+\frac{1}{D}\iint_R\Phi(x,y;\xi,\eta)\left[w_1(x,y)\frac{U(x,y)}{\partial x}+w_2(x,y)\frac{U(x,y)}{\partial y}\right]dxdy-\frac{\Phi(x,y;\xi,\eta)G(x,y)}{D} \quad (4)$$

with

$$\lambda(\xi,\eta)=\begin{cases}1,(\xi,\eta)\in R,\\ \frac{1}{2},(\xi,\eta)\in C\end{cases}$$

and

$\Phi(x,y;\xi,\eta)=\frac{1}{4\pi}\ln[(x-\xi)^2+(y-\eta)^2]$ is the two-dimensional Laplace basic solution. From Eqs. (3) and (4), the following system of linear equations is obtained.

$$\lambda^{(n)}U^{(n)}=\sum_{k=1}^{N}\left[U^{(k)}\int_{C^{(k)}}\frac{\Phi(x,y;\xi,\eta)}{\partial n}ds-p^{(k)}\int_{C^{(k)}}\Phi(x,y;\xi,\eta)ds\right]$$
$$+\sum_{i=1}^{N+L}w_1^{(n)}\mu_x^{(ni)}+w_2^{(n)}\mu_y^{(ni)}-\sum_{i=1}^{N+L}\mu^{(ni)}G\left(x^{(i)},y^{(i)}\right), \quad (5)$$

$n=1,2,3,\dots,N+L,$

and

$$\lambda^{(n)}U^{(n)}=\sum_{k=1}^{N}\left[U^{(k)}\int_{C^{(k)}}\frac{\Phi(x,y;\xi,\eta)}{\partial n}ds-p^{(k)}\int_{C^{(k)}}\Phi(x,y;\xi,\eta)ds\right]$$
$$+\sum_{i=1}^{N+L}w_1^{(n)}\mu_x^{(ni)}+w_2^{(n)}\mu_y^{(ni)}-\Phi\left(x,y;x^{(n)},y^{(n)}\right)G(a,b), \quad (6)$$

$n=1,2,3,\dots,N+L.$

Here the $N$ notation denotes the number of boundary segments. The notations $C,C^{(1)},C^{(2)},C^{(3)},C^{(4)},\dots,C^{(N)}$ denotes the segment amount. Those segments satisfy $C=C^{(1)}\cup C^{(2)}\cup C^{(3)}\cup C^{(4)}\cup\dots\cup C^{(N)}$. Also, notation $L$ denotes the number of interior interpolation points. Points $\left(x^{(1)},y^{(1)}\right),\left(x^{(2)},y^{(2)}\right),\left(x^{(3)},y^{(3)}\right),\dots,\left(x^{(N)},y^{(N)}\right)$ are the middle points of every segment of $C^{(1)},C^{(2)},\dots,C^{(N)}$. Points $\left(x^{(N+1)},y^{(N+1)}\right),\left(x^{(N+2)},y^{(N+2)}\right),\left(x^{(3)},y^{(3)}\right),\dots,\left(x^{(N+L)},y^{(N+L)}\right)$ are interior interpolation points.

$\lambda^{(n)}=\lambda\left(x^{(n)},y^{(n)}\right),$

$U^{(n)}=U\left(x^{(n)},y^{(n)}\right),$

$p^{(n)}=\frac{\partial T}{\partial n}\Big|\,(x,y)=\left(x^{(n)},y^{(n)}\right),$

$w_1^{(n)}=w_1\left(x^{(n)},y^{(n)}\right),$

$w_2^{(n)}=w_2\left(x^{(n)},y^{(n)}\right),$

$\mu_x^{(ni)} = \sum_{j=1}^{N+L} \mu^{ni} \frac{\partial \rho(x,y;x^{(j)},y^{(j)})}{\partial x}\Big|_{(x,y)=(x^{(i)},y^{(i)})} \times \rho^{-1}(x^{(i)},y^{(i)};x^{(j)},y^{(j)}),$

$\mu_y^{(ni)} = \sum_{j=1}^{N+L} \mu^{ni} \frac{\partial \rho(x,y;x^{(j)},y^{(j)})}{\partial y}\Big|_{(x,y)=(x^{(i)},y^{(i)})} \times \rho^{-1}(x^{(i)},y^{(i)};x^{(j)},y^{(j)}),$

$\mu^{(ni)} = \sum_{j=1}^{N+L} \psi^{(nj)} \rho^{-(ij)},$

$\psi^{(nj)} = \lambda(x^{(n)},y^{(n)})\chi(x^{(n)},y^{(n)};x^{(j)},y^{(j)}) + \int_C \left[\Phi(x,y;x^{(n)},y^{(n)}) \frac{\partial \chi(x,y;x^{(j)},y^{(j)})}{\partial n} - \frac{\chi(x,y;x^{(j)},y^{(j)})\Phi(x,y;x^{(n)},y^{(n)})}{\partial n}\right] ds\,,$

where $\rho$ is a polynomial function defined as

$$\rho = 1 + r^2 + r^3, \text{ and } \chi = \frac{1}{4}r^2 + \frac{1}{16}r^4 + \frac{1}{25}r^5.$$

Function $r$ is the Euclidean distance formula defined as

$$r(x,y;\alpha,\beta) = \sqrt{(x-\alpha)^2 + (y-\beta)^2}.$$

Subsequently, the system of linear algebraic equations given by Eqs. (5) and (6) is solved, yielding numerical solutions at the interpolation points. Using this numeric solution at interpolation points, then the numeric solution at any $(\alpha,\beta) \in R \cup C$ can be obtained via the following expression.

$$\begin{aligned}\lambda(\alpha,\beta)\quad U(\alpha,\beta) \quad &= \sum_{k=1}^{N}\left[U^{(k)} \int_{C^{(k)}} \frac{\Phi(x,y;\xi,\eta)}{\partial n} ds - p^{(k)} \int_{C^{(k)}} \Phi(x,y;\xi,\eta) ds\right] \\ &+ \sum_{i=1}^{N+L} w_1^{(n)} \mu_x^{(ni)} + w_2^{(n)} \mu_y^{(ni)} - \Phi(x,y;x^{(n)},y^{(n)}) G(\alpha,\beta)\end{aligned}$$

## 3. RESULTS AND DISCUSSION

This section presents the numerical results obtained using the Dual Reciprocity Boundary Element Method (DRBEM) for the convection-diffusion equation. Two test cases are examined. First, a convection-diffusion problem with a known analytical solution is considered to validate the accuracy of the numerical method (Section 3.1). Subsequently, the method is applied to a real-world problem involving steady material dispersion with three-point sources in a reservoir (Section 3.2) to demonstrate its practical applicability.

### 3.1 A Convection-diffusion Problem with Analytic Solution

This section presents a simple example of the Convection-diffusion Equation. The aim is to obtain both the analytical and numeric solutions in order to evaluate how well the numeric approach approximates the analytical solution. DRBEM is utilized to compute the numeric solution. The form of the simplified Convection-diffusion Equation to be solved is given by Eq. (7).

$$\frac{\partial U(x,y)}{\partial x} w_1(x,y) + \frac{\partial U(x,y)}{\partial y} w_2(x,y) - D\left(\frac{\partial^2 U(x,y)}{\partial x^2} + \frac{\partial^2 U(x,y)}{\partial y^2}\right) = g(x,y), \qquad (7)$$

with

$$w_1(x,y) = y^2, w_2(x,y) = x^2, D = 1$$

and

$$g(x,y) = 2xy^2 + 2x^2y - 4.$$

The problem is outlined over a closed rectangle domain, with boundary conditions (BC) specified as illustrated in Fig. 1.

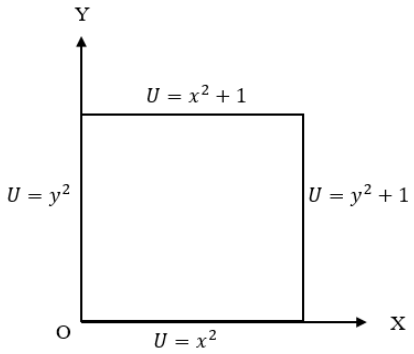


**Figure 1. Region and BC of Convection-Diffusion**

The analytical solution of Eq. (7) with the BC described above is

$$U(x, y) = x^2 + y^2.$$

Subsequently, DRBEM is applied to compute the numeric solution. The interpolation points are selected and grouped into two sets, denoted by Set A and Set B. Set A consists of 100 segment elements and 81 interior interpolation points, while Set B comprises 200 segment elements and 196 interpolation points. This selection is based on an even distribution across the four boundary curves and interior points spread evenly across a region whose number can be expressed as a quadratic number. Error value in Set A is denoted by $e_A$, and the error value in Set B is denoted by $e_B$. The results of the analytical and numerical calculations for Sets A and B obtained using MATLAB are presented in Table 1 and Table 2, respectively. The points shown in Table 1 are interior interpolation points distributed uniformly across the domain with a spacing of 0.20 units in both x and y directions.

**Table 1. Analytic and Numeric Value of Set A**

| Point | Set A | Analytic | $e_A$ |
|---|---|---|---|
| (0.20,0.20) | 0.0804032621 | 0.0800000000 | 0.0004032621 |
| (0.40,0.20) | 0.1930923968 | 0.2000000000 | 0.0069076032 |
| (0.60,0.20) | 0.3865181089 | 0.4000000000 | 0.0134818911 |
| (0.80,0.20) | 0.6635903906 | 0.6800000000 | 0.0164096094 |
| (0.20,0.40) | 0.2077248968 | 0.2000000000 | 0.0077248968 |
| (0.40,0.40) | 0.3204095595 | 0.3200000000 | 0.0004095595 |
| (0.60,0.40) | 0.5138098964 | 0.5200000000 | 0.0061901036 |
| (0.80,0.40) | 0.7883387530 | 0.8000000000 | 0.0116612470 |
| (0.20,0.60) | 0.4143096490 | 0.4000000000 | 0.0143096490 |
| (0.40,0.60) | 0.5270127464 | 0.5200000000 | 0.0070127464 |
| (0.60,0.60) | 0.7204103072 | 0.7200000000 | 0.0004103072 |
| (0.80,0.60) | 0.9911987060 | 1.0000000000 | 0.0088012940 |
| (0.20,0.80) | 0.6972388725 | 0.6800000000 | 0.0172388725 |
| (0.40,0.80) | 0.8124828486 | 0.8000000000 | 0.0124828486 |
| (0.60,0.80) | 1.0096167138 | 1.0000000000 | 0.0096167138 |
| (0.80,0.80) | 1.2804017239 | 1.2800000000 | 0.0004017239 |

**Table 2. Analytic and Numeric Value of Set B**

| Point | Set B | Analytic | $e_B$ |
|---|---|---|---|
| (0.20,0.20) | 0.0801006880 | 0.0800000000 | 0.0001006880 |
| (0.40,0.20) | 0.1964275931 | 0.2000000000 | 0.0035724069 |
| (0.60,0.20) | 0.3931405615 | 0.4000000000 | 0.0068594385 |
| (0.80,0.20) | 0.6716924803 | 0.6800000000 | 0.0083075197 |
| (0.20,0.40) | 0.2037764295 | 0.2000000000 | 0.0037764295 |
| (0.40,0.40) | 0.3201027148 | 0.3200000000 | 0.0001027148 |
| (0.60,0.40) | 0.5167923916 | 0.5200000000 | 0.0032076084 |
| (0.80,0.40) | 0.7940475696 | 0.8000000000 | 0.0059524304 |
| (0.20,0.60) | 0.4070653515 | 0.4000000000 | 0.0070653515 |
| (0.40,0.60) | 0.5234146429 | 0.5200000000 | 0.0034146429 |

| Point | Set B | Analytic | $e_B$ |
|---|---|---|---|
| (0.60,0.60) | 0.7201042228 | 0.7200000000 | 0.0001042228 |
| (0.80,0.60) | 0.9954712790 | 1.0000000000 | 0.0045287210 |
| (0.20,0.80) | 0.6885144728 | 0.6800000000 | 0.0085144728 |
| (0.40,0.80) | 0.8061608098 | 0.8000000000 | 0.0061608098 |
| (0.60,0.80) | 1.0047381848 | 1.0000000000 | 0.0047381848 |
| (0.80,0.80) | 1.2801044672 | 1.2800000000 | 0.0001044672 |

Based on the results presented in Table 1 and Table 2 above, a comparison between the numeric solutions/values of Set A and Set B can be obtained. For Set A, the supreme value of error is 0.0172388725, whereas Set B yields a lower supreme error value, that is 0.0085144728. This significant reduction in error indicates that Set B achieves a more accurate approximation of the analytical solution. The key difference between the two sets lies in the number of interpolation points used. Set B employs a larger amount of interpolation points, which enhances the resolution of the numeric method. Therefore, it can be inferred that increasing the number of interpolation points leads to improved numeric accuracy.

Next, the figures of the numeric surface plot will be shown in Fig. 2 and Fig. 3.

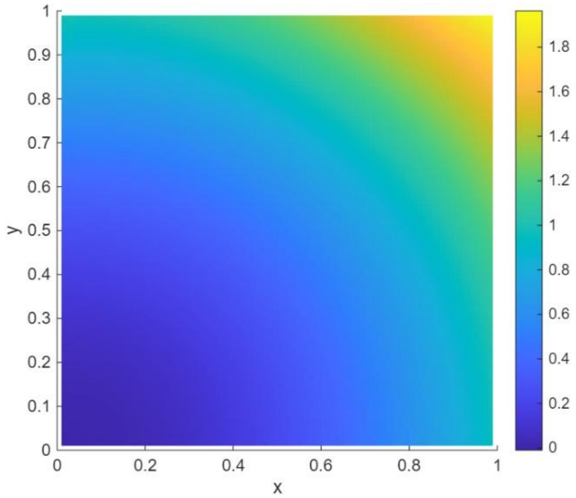


**Figure 2. Numeric Result of Set A**

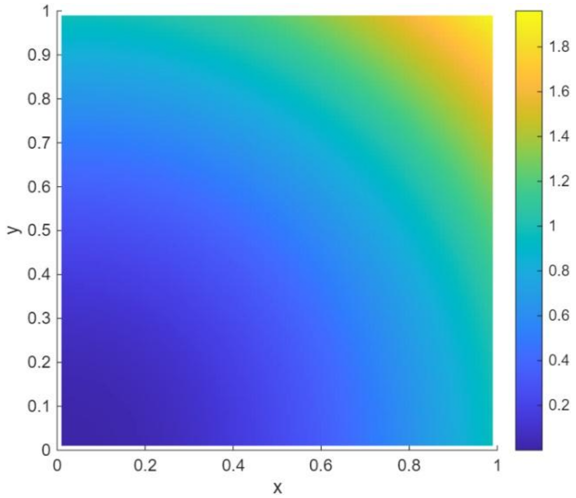


**Figure 3. Numeric Result of Set B**

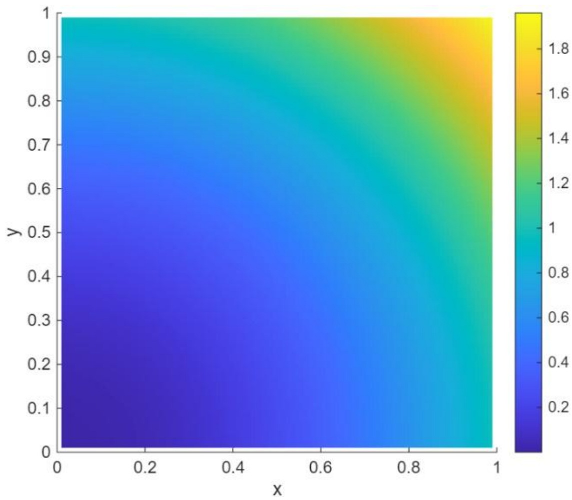


**Figure 4.** **Analytical Values**

The numerical surface plots are presented in Fig. 2 and Fig. 3, while Fig. 4 displays the analytical surface plot. The numerical plots exhibit strong similarity to the analytical plot, which is consistent with the values presented in Table 1 and Table 2. In all three figures, the color gradient from blue to yellow indicates an increase in the value of $U$, ranging from 0.2 to 1.8. No visible differences can be distinguished among the three plots due to the close agreement between the numerical and analytical values. This observation is consistent with the results in Table 1 and Table 2, where the error at each selected point demonstrates relatively small values. In general, the more collocation points we choose, the closer the numerical solution will be to the exact solution. This is because more boundary collocation points will result in a smoother approximation of the boundary curve, and more interior collocation points will result in clearer exact conditions in the region being described.

### 3.2 Steady Material Dispersion with Three-Point Bases in The Reservoir

Moreover, DRBEM is applied to the dispersion of material in a reservoir with three bases. To investigate the effect of source positioning, the relative distance between the two bases was systematically varied. The ten test cases in Table 3 were designed to evaluate the method's performance under different source point configurations. Cases 1-4 examine vertically and horizontally aligned sources, Cases 5-8 investigate corner and boundary placements, and Cases 9-10 assess diagonal distributions. These configurations simulate various realistic scenarios of pollutant source placement. Table 3 summarizes the different point locations used in the study. In addition, the diffusion coefficient is $D = 11.75$ m$^2$/s and the value of the concentration on each base is constant 25/107 gram/s.

**Table 3.** **Variation of Source Locations**

| Case | Points Location |
|---|---|
| Case 1 | (40,40), (40,24), (40,8) |
| Case 2 | (52,8), (52,24), (52,40) |
| Case 3 | (28,8), (28,24), (28,40) |
| Case 4 | (28,24), (40,24), (52,24) |
| Case 5 | (28,8), (52,8), (52,40) |
| Case 6 | (28,8), (28,40), (52,40) |
| Case 7 | (28,40), (28,8), (52,8) |
| Case 8 | (28,40), (52,40), (52,8) |
| Case 9 | (52,40), (40,24), (28,8) |
| Case 10 | (28,40), (40,24), (52,8) |

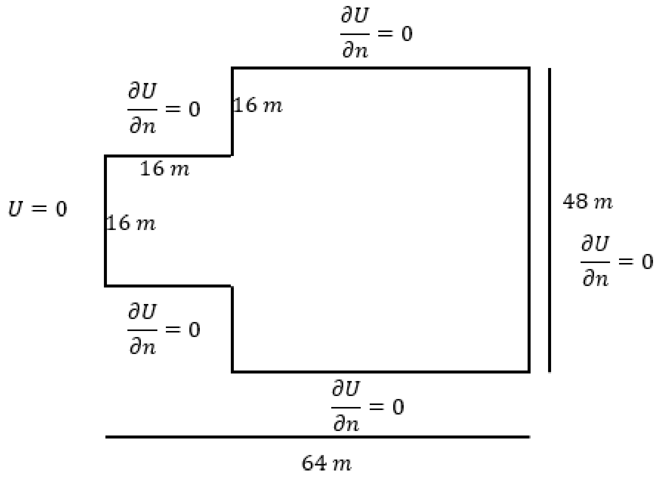


**Figure 5.** **Region and Boundary Conditions**

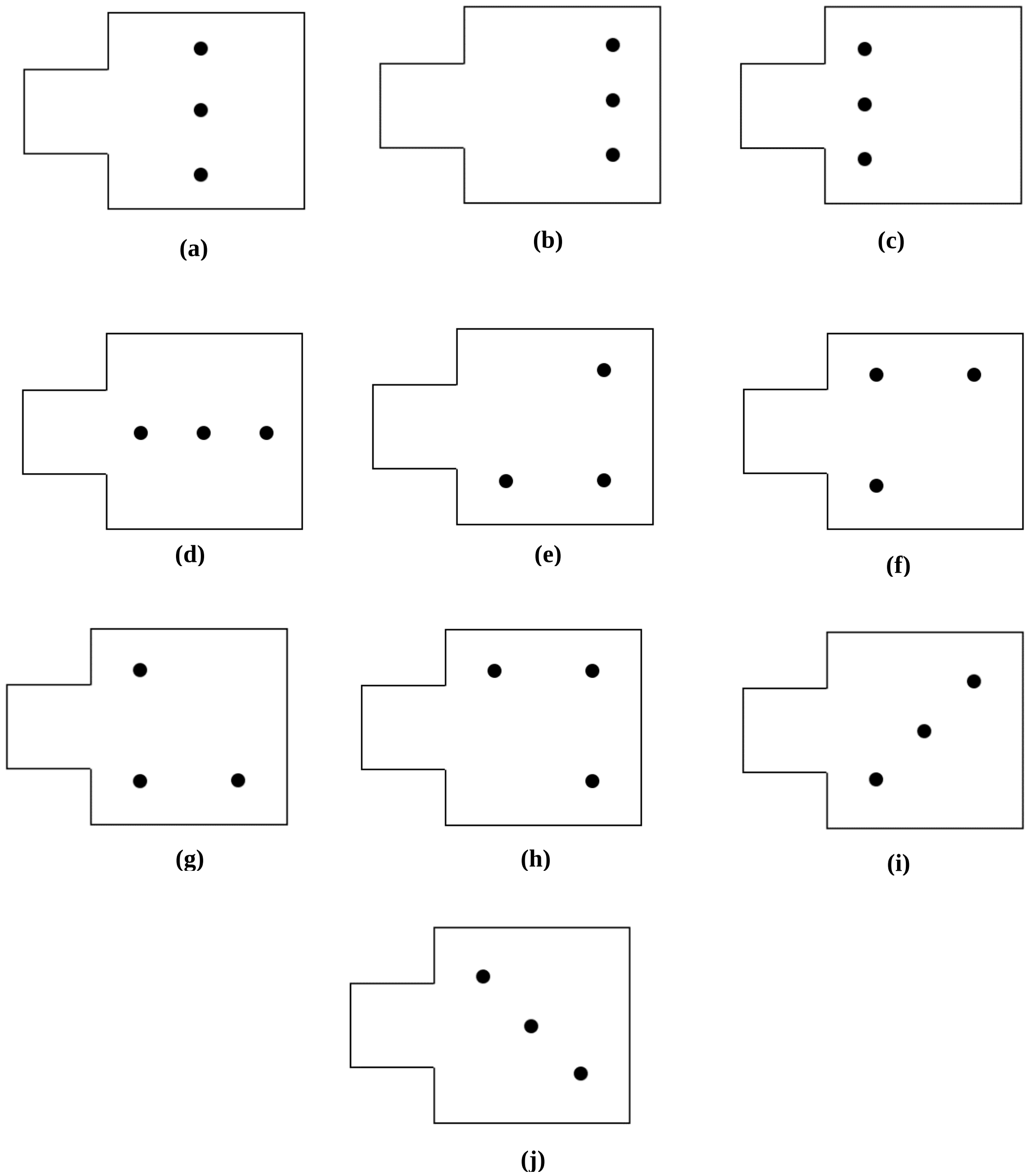

**Figure 6.** **Point location variations for Cases 1–10 (a–j)**

Fig. 6 illustrates the geometric configurations of three-point sources for all ten test cases: (a–d) aligned arrangements, (e–h) corner placements, and (i–j) diagonal distributions. All cases are simulated within a reservoir domain with a width of 48 m. The upstream boundary is set with the condition $U = 0$ while the remaining boundaries follow the condition $\frac{\partial U}{\partial n} = 0$. Before applying the DRBEM, the velocity components $w_x$ and $w_y$ are determined at the interior interpolation points, with the supreme inflow velocity being 0.150 m/s. The $k$-epsilon turbulence model is used by fixing a system of governing equations.

$$\frac{\partial w_x}{\partial x} + \frac{\partial w_y}{\partial y} = 0,$$

$$w_x \frac{\partial w_x}{\partial x} + w_y \frac{\partial w_x}{\partial y} = -\frac{1}{\rho}\frac{\partial \rho}{\partial x} + \gamma\left(\frac{\partial^2 w_x}{\partial x^2} + \frac{\partial^2 w_x}{\partial y^2}\right),$$

$$w_x \frac{\partial w_y}{\partial x} + w_y \frac{\partial w_y}{\partial y} = -\frac{1}{\rho}\frac{\partial \rho}{\partial y} + \gamma\left(\frac{\partial^2 w_y}{\partial x^2} + \frac{\partial^2 w_y}{\partial y^2}\right),$$

$$\frac{\partial}{\partial x}\left(\frac{w_t}{\sigma_k}\frac{\partial_k}{\partial x}\right) = \varepsilon - P_k,$$

$$\frac{\partial}{\partial y}\left(\frac{w}{\sigma_k}\frac{\partial_k}{\partial y}\right) = \varepsilon - P_k,$$

$$\frac{\partial}{\partial x}\left(\frac{w_t}{\sigma_\varepsilon}\frac{\partial_\varepsilon}{\partial x}\right) = C_{\varepsilon 2}\frac{\varepsilon^2}{k} - C_{\varepsilon 1}\frac{\varepsilon}{k}P_k,$$

$$\frac{\partial}{\partial y}\left(\frac{w_t}{\sigma_\varepsilon}\frac{\partial_\varepsilon}{\partial y}\right) = C_{\varepsilon 2}\frac{\varepsilon^2}{k} - C_{\varepsilon 1}\frac{\varepsilon}{k}P_k,$$

where $w_t = C_\mu \frac{k^2}{\varepsilon}; P_k = \frac{1}{2} w_t \left(\frac{\partial \overrightarrow{w_x}}{\partial y} \frac{\partial \overrightarrow{w_y}}{\partial x}\right); C_\mu = 0.09; C_{\varepsilon 1} = 1.44; C_{\varepsilon 2} = 1.92;\ \sigma_k = 1.00,; \sigma_\epsilon = 1.30, \overrightarrow{w_t}$ is shear tension with respect to $i$ direction, $\rho$ is density, $\gamma$ is kinematic viscosity and $p$ is pressure. The result of the velocity profile is shown in Fig. 7. The profile of velocity is attained using software *ANSYS 19.2* from the previous study by Ashar and Hariyanto [8]. The resulting data velocity profile can be directly adapted to this paper, because the shape of the reservoir used is the same, as are the turbulent flow conditions. The only difference is the use of three source points, whereas the previous study used only two source points.

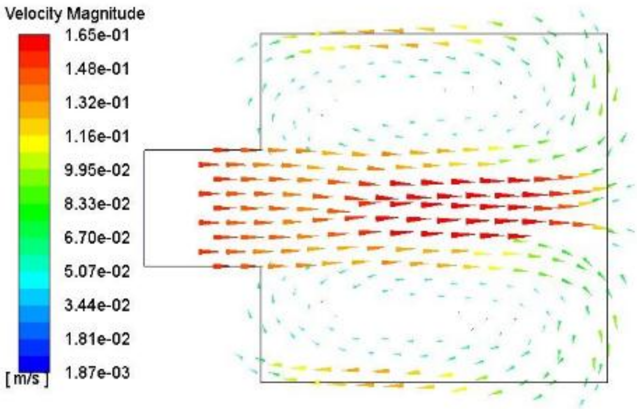


**Figure 7. Visual of Velocity Profile**

To enable a more detailed argument, the distribution habit of the material across lines $l_1$ and $l_2$ is examined across all Cases. Line $l_1$ represents a vertical axis that bisects the main section of the reservoir into two equal halves, while line $l_2$ serves as a horizontal axis that similarly splits the reservoir evenly. Illustration of lines $l_1$ and $l_2$ are shown in Fig. 8.

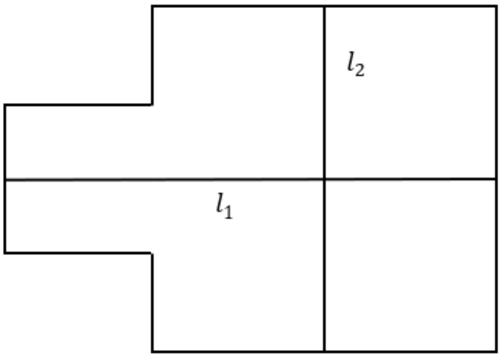


**Figure 8. Illustrations of Line $l_1$ and $l_2$**

Then the entire concentration of the material across line $l_1$, $l_2$, and the entire region is calculated. For across line $l_1$ and $l_2$, $\int_{l_i} U(x,y)ds,\ \ i = 1,2$ is calculated. For entire region, $\iint_R U(x,y)dxdy$ is computed. The numerical results for all test cases are summarized in Table 4.

**Table 4. Aggregate Concentration Across $l_1$, $l_2$, and the Entire Region Corresponding to 200 Segments and 196 Interior Collocation Points**

| Source | Across $l_1$ | Across $l_2$ | Entire Region |
|---|---|---|---|
| Case 1 | 440.16 mg | 591.43 mg | 47864.62 mg |
| Case 2 | 459.78 mg | 590.00 mg | 50135.70 mg |
| Case 3 | 405.84 mg | 517.37 mg | 43931.57 mg |
| Case 4 | 448.31 mg | 561.51 mg | 46918.56 mg |
| Case 5 | 434.79 mg | 567.64 mg | 48209.97 mg |
| Case 6 | 419.08 mg | 546.26 mg | 46397.33 mg |
| Case 7 | 419.09 mg | 546.28 mg | 46398.39 mg |
| Case 8 | 434.73 mg | 567.57 mg | 48203.58 mg |
| Case 9 | 436.57 mg | 568.04 mg | 47458.58 mg |
| Case 10 | 436.52 mg | 567.98 mg | 47453.27 mg |

In Table 4, the combined uniformity score S is used, which multiplies the total accumulation across the entire domain by the cross-sectional uniformity index between $l_1$ and $l_2$. In this paper, $J_{l1}$ and $J_{l2}$ are total concentration value along the line $l_1$ and $l_2$. Next, compute $B = \frac{|J_{l1} - J_{l2}|}{(J_{l1} + J_{l2})/2}$, uniformity index $UI = 1 - B$, thus $E = \left(\iint_R UdA\right)(1 - B)$ represents the total effective mass distributed evenly (large if the total is high and the concentration difference is integrated on both small lines). Based on these calculations, Case 2 yields the highest score $E = 37{,}697.53$, thus being identified as the configuration with the most uniform distribution overall according to this combined metric; on average, Case 2 is ~8.53% better than the other Cases (Case 1 and 3–10), with an improvement range of approximately 3.57% to 13.15%. Below are numeric surface plots of material dispersion in a reservoir for better illustration.

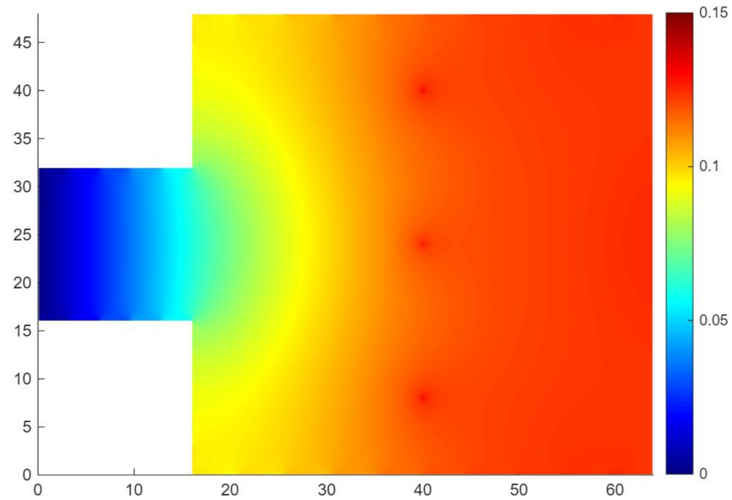

**Figure 9.** Surface Plot Case 1

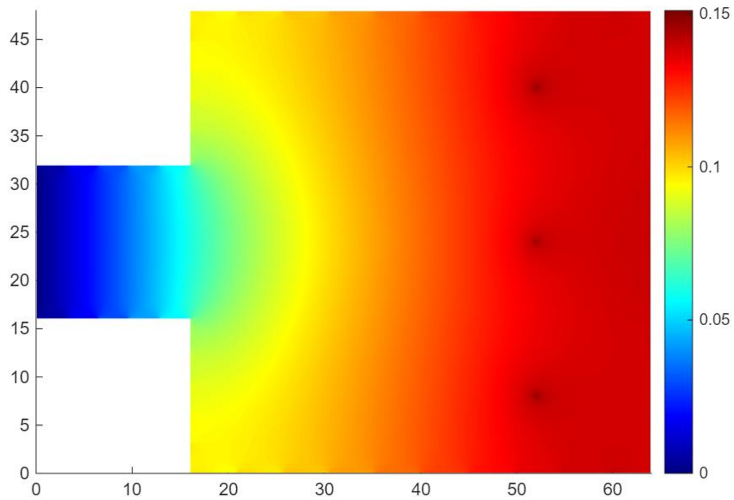

**Figure 10.** Surface Plot Case 2

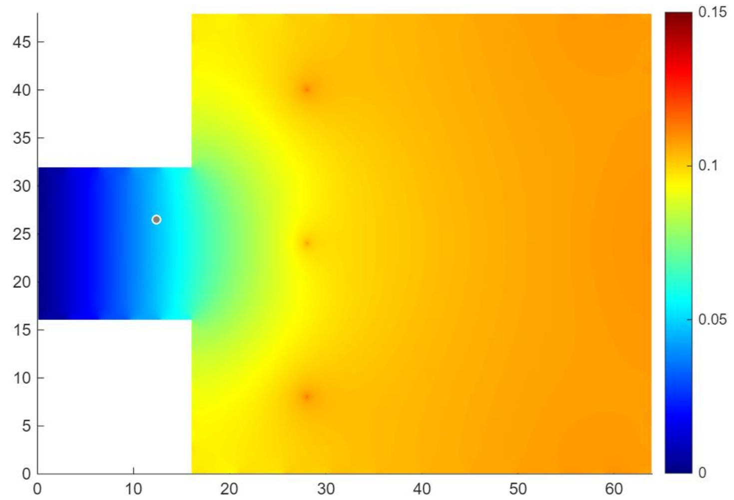

**Figure 11.** Surface Plot Case 3

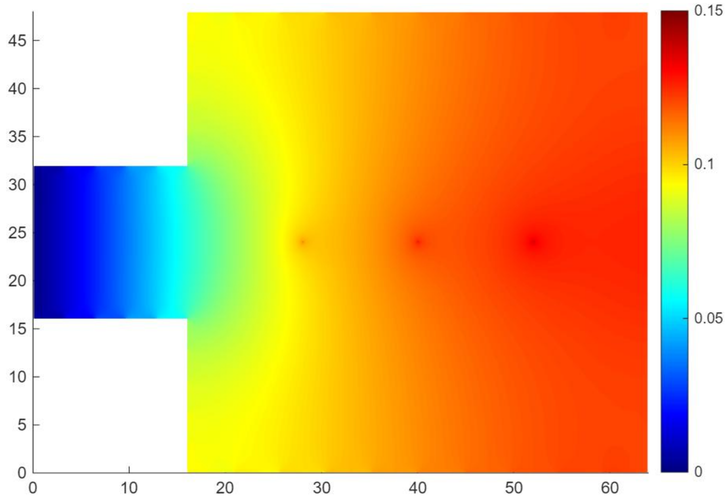


Figure 12. Surface Plot Case 4

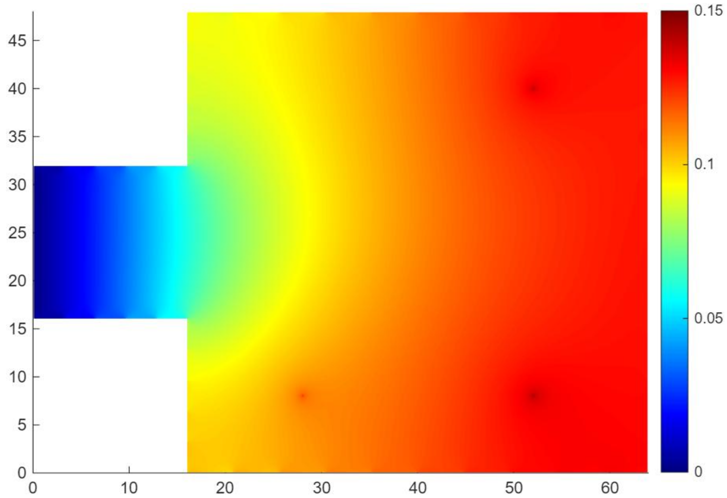


Figure 13. Surface Plot Case 5

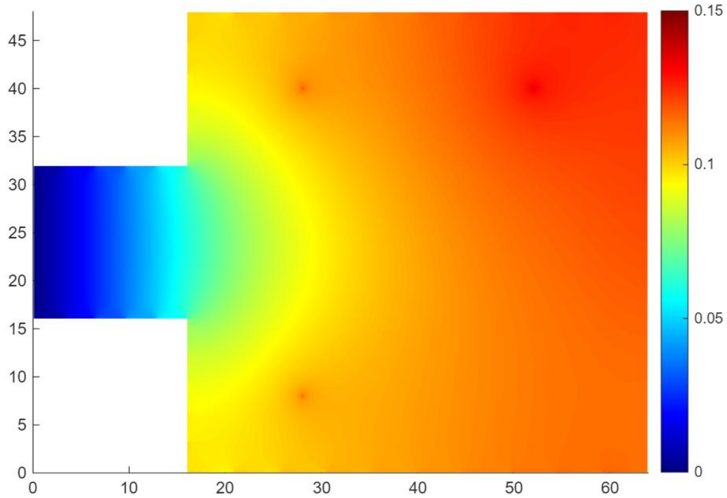


Figure 14. Surface Plot Case 6

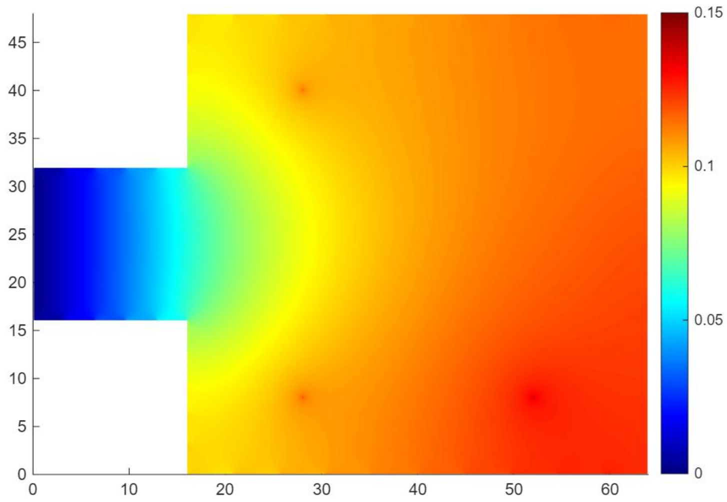


**Figure 15.** Surface Plot Case 7

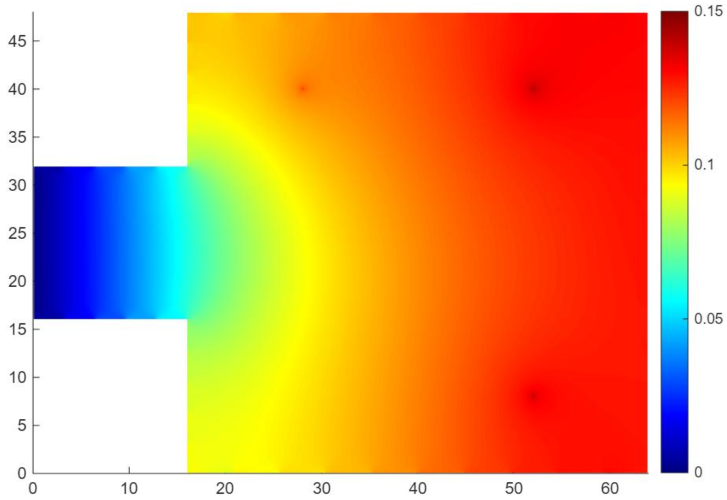


**Figure 16.** Surface Plot Case 8

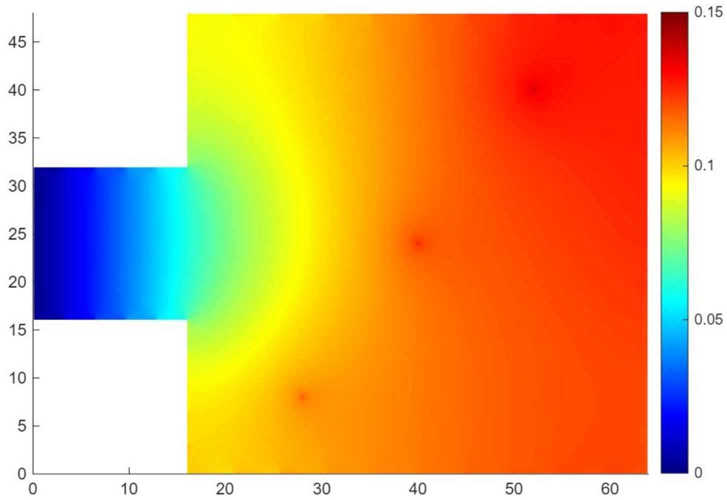


**Figure 17.** Surface Plot Case 9

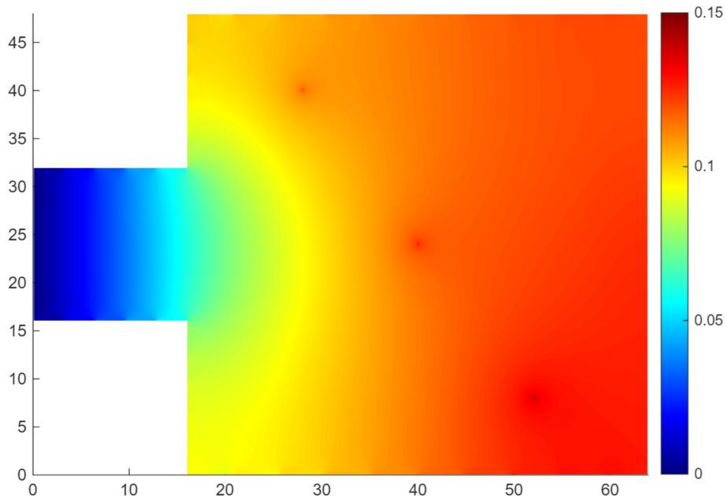


**Figure 18. Surface Plot Case 10**

Fig. 9 to Fig. 18 above show the effect of placing the three source positions in the region. Ten test cases were designed to demonstrate the patterns of material dispersion behavior in the region. In general, the concentration values around the points will show fairly high amounts, while concentration values farther from the source points will show a decrease. Visual inspection of the ten figures alone does not allow for definitive determination of which configuration yields the most optimal material distribution; quantitative assessment requires numerical calculation using an integral approach. There is something interesting about the ten images above, namely the presence of a yellow line shaped like a parabola, which is influenced by the positions of the three source points.

On the other hand, Table 4 also implies that a higher total accumulation of substances (such as cleaning/purifying agents) in reservoirs will generally increase reservoir performance because it can improve water quality (eutrophication/dissolved oxygen), reduce treatment requirements and operational risks (sedimentation/corrosion/biofouling), thereby increasing the efficiency of water storage, distribution, and utilization functions. Physically and in relation to the previous velocity profile results, Case 2 shows the best results because the points are on the downstream side (right), in the same direction as the advection/convection. In convective flow, momentum/scalar transport is predominantly carried from the inlet to the outlet; thus, placing points downstream captures conditions that are already the result of flow evolution throughout the domain (accumulation of shear effects, diffusion, and streamline deflection). In other words, this is most consistent with flow causality (information from upstream affects downstream). Therefore, sampling/constraints downstream is more effective for representing the overall solution.

Additionally, the velocity profile in the figure shows maximum velocity in the central corridor and recirculation zones (vortices) at the top and bottom. The vertical arrangement of points in Case 2 intersects several streamlines in the top, middle, and bottom sections, capturing the strong velocity gradient between the fast flow in the middle and the slower/rotating flow near the wall. Since the greatest heterogeneity (shear layer) occurs at this transition, Case 2 provides a more complete representation of the flow direction and velocity magnitude variation than other Cases that focus only on one zone. This is not found in any of the other Cases.

## 4. CONCLUSION

From the research that has been conducted, three conclusions were found, namely:

1. DRBEM has been successfully applied to the convection-diffusion equation with three source points. This method is used to determine which combination of the three source point locations has the greatest influence on the total concentration of the material. Ten source point configurations, designated as Cases 1–10, were examined.
2. Before using DRBEM, the velocity profile must be obtained. In this paper, the velocity profile obtained from a study conducted by Ashar and Hariyanto [8]. After that, DRBEM can be applied in every Case

to find the numeric results. The results indicate that Case 2 achieved approximately 8.53% higher uniformity compared to the other cases. Therefore, it can be concluded that the source point configuration used in Case 2 promotes more effective material dispersion. This shows results that are consistent with the previous study by Ashar and Hariyanto [8], that placing bases like Case 2 or at the back of the reservoir is the most effective for material distribution.

3. These results demonstrate that DRBEM is a reliable approach for evaluating source placement in diffusion–convection problems and can provide practical guidance for optimizing material distribution in similar systems. The above results are supported by a study of river confluence at the Riba-Roja Reservoir, which confirms that the processes within the reservoir develop in accordance with advection (carried by the flow), so that observations/placement of points aligned with the direction of flow (downstream) are more representative [20]. However, the present study is limited to a single velocity profile and specific boundary conditions; further research could investigate different flow patterns, varying amounts of bases, or comparisons with other numerical methods to enhance the generality of these conclusions.

## Author Contributions

Nurcahya Yulian Ashar: Conceptualization, methodology, validation. Muhammad Manaqib: Writing-review & editing, rebases, draft preparation, validation. Yoga Amanda Putra: Writing—original draft, software, proper analysis. All authors considered the findings and provided input for the final manuscript.

## Funding Statement

This research received no specific grant from any funding agency in the public, commercial, or not-for-profit sectors.

## Acknowledgment

We would like to express our gratitude to UIN Syarif Hidayatullah Jakarta and Selain APBN FSM Undip number 31.B/UN7.F8/PP/II/2026 for their support in this research.

## Declarations

The authors state that he has no bias-related issues to report in the study.

## Declaration of Generative AI and AI-assisted Technologies

Generative AI tools (e.g., ChatGPT) were used solely for language refinement, including grammar, spelling, and clarity. The scientific content, analysis, interpretation, and conclusions were developed entirely by the authors. All final text was reviewed and approved by the authors.

## REFERENCES

[1] L. Samec, Niko, and Skerget, “NUMERICAL MODELLING OF POLLUTANT DISPERSION IN WATER SYSTEMS,” *WIT Press*, vol. 32, 1998.

[2] M. Stynes, “STEADY-STATE CONVECTION-DIFFUSION PROBLEMS,” Acta Numerica, vol. 14, pp. 445–508, 2005. doi: https://doi.org/10.1017/S0962492904000261.

[3] V.F. Morales-Delgado, J.F. Gómez-Aguilar, and M.A. Taneco-Hernandez, “ANALYTICAL SOLUTION OF THE TIME FRACTIONAL DIFFUSION EQUATION AND FRACTIONAL CONVECTION-DIFFUSION EQUATION,” *Rev. Mex. física*, vol. 65, pp. 82–88, 2019. doi: https://doi.org/10.31349/RevMexFis.65.82.

[4] A. D. Polyanin, “FUNCTIONAL SEPARABLE SOLUTIONS OF NONLINEAR CONVECTION–DIFFUSION EQUATIONS WITH VARIABLE COEFFICIENTS,” *Commun. Nonlinear Sci. Numer. Simul.*, vol. 73, pp. 379–390, 2019. doi: https://doi.org/10.1016/j.cnsns.2019.02.022.

[5] M. Zhang, W. Zhao, and P. Lin, “LATTICE BOLTZMANN METHOD FOR GENERAL CONVECTION-DIFFUSION EQUATIONS: MRT MODEL AND BOUNDARY SCHEMES,” *J. Comput. Phys.*, vol. 389, pp. 147–163, 2019. doi: https://doi.org/10.1016/j.jcp.2019.03.045.

[6] F. Wang, C.M. Fan, C. Zhang, and J. Lin, “A LOCALIZED SPACE-TIME METHOD OF FUNDAMENTAL SOLUTIONS FOR DIFFUSION AND CONVECTION-DIFFUSION PROBLEMS,” *Adv. Appl. Math. Mech.*, vol. 12, no. 4, pp. 940–958, 2020. doi: https://doi.org/10.4208/aamm.OA-2019-0269.

[7] J.H. He, "A SIMPLE APPROACH TO ONE-DIMENSIONAL CONVECTION-DIFFUSION EQUATION AND ITS FRACTIONAL MODIFICATION FOR E REACTION ARISING IN ROTATING DISK ELECTRODES," *J. Electroanal. Chem.*, vol. 854, p. 113565, 2019. doi: https://doi.org/10.1016/j.jelechem.2019.113565.

[8] N. Y. Ashar and S. Hariyanto, "A NUMERICAL STUDY OF SUBSTANCE SPREAD IN THE POOL FROM TWO POINT SOURCES," *Barekeng*, vol. 17, pp. 9--20, 2023. doi: https://doi.org/10.30598/barekengvol17iss1pp0009-0020.

[9] S. A. Al-Bayati and L. C. Wrobel, "TRANSIENT CONVECTION-DIFFUSION-REACTION PROBLEMS WITH VARIABLE VELOCITY FIELD BY MEANS OF DRBEM WITH DIFFERENT RADIAL BASIS FUNCTIONS," in Computational and Analytic Methods in Science and Engineering, C. Constanda, Ed. Cham, Switzerland: Birkhäuser, 2020. doi: https://doi.org/10.1007/978-3-030-48186-5_2.

[10] M. Manaqib, "DUAL RECIPROCITY BOUNDARY ELEMENT METHOD UNTUK MENYELESAIKAN MASALAH INFILTRASI SALURAN IRIGASI ALUR DI DALAM BEBERAPA JENIS TANAH HOMOGEN," *Univ. Gadjah Mada*, 2015.

[11] D. L. Clements and M. Lobo, "A BEM FOR TIME DEPENDENT INFILTRATION FROM AN IRRIGATION CHANNEL," *Eng. Anal. Bound. Elem.*, vol. 34, no. 12, pp. 1100–1104, 2010. doi: https://doi.org/10.1016/j.enganabound.2010.06.013.

[12] I. Solekhudin and K.C. Ang, "A LAPLACE TRANSFORM DRBEM WITH A PREDICTOR–CORRECTOR SCHEME FOR TIME-DEPENDENT INFILTRATION FROM PERIODIC CHANNELS WITH ROOT-WATER UPTAKE," *Eng. Anal. Bound. Elem.*, vol. 50, pp. 141–147, 2015. doi: https://doi.org/10.1016/j.enganabound.2014.08.011

[13] I. Solekhudin, "A NUMERICAL METHOD FOR TIME-DEPENDENT INFILTRATION FROM PERIODIC TRAPEZOIDAL CHANNELS WITH DIFFERENT TYPES OF ROOT-WATER UPTAKE.," *IAENG Int. J. Appl. Math.*, vol. 48, no. 1, p. 84, 2018. doi: https://doi.org/10.2991/icomse-17.2018.6.

[14] A. Munadi, I. Solekhudin, Sumardi, A. Zulijanto, "A NUMERICAL STUDY OF STEADY INFILTRATION FROM A SINGLE IRRIGATION CHANNEL WITH AN IMPERMEABLE SOIL LAYER.," *Eng. Lett.*, vol. 28, no. 3, p. 643, 2020.

[15] N. Y. Ashar, "AN APPLICATION OF DUAL RECIPROCITY BOUNDARY ELEMENT METHOD ON CALCULATION OF POLLUTANT CONCENTRATION RANGE IN TWINNED PATH WITH LAMINAR WATER FLOW," *Univ. Gadjah Mada*, 2020.

[16] N.Y. Ashar, I. Solekhudin, "A Numerical Study of Steady Pollutant Spread in Water from a Point Source.," *Eng. Lett.*, vol. 29, no. 3, p. 840, 2021.

[17] N. Alsoy-Akgün, "NATURAL CONVECTION RESULTING FROM EXPONENTIALLY VARYING WALL HEATING IN A SQUARE ENCLOSURE," *Comput. Math. with Appl.*, vol. 197, pp. 235–258, 2025. doi: https://doi.org/10.1016/j.camwa.2025.08.024.

[18] M. Zahroh, D. I. Pramadhani, and M. Hasan, "Implementation of DRBEM with predictor-corrector for infiltration in four layered heterogeneous soil under impermeable and non-impermeable conditions," *Stat., optim. inf. Comput.*, 2025. doi: https://doi.org/10.19139/soic-2310-5070-2376.

[19] P. Priya, Vinita, P. Kumar, R. Prasad, Y. Hisaki, and Rajni, "Assessing wave energy spectra at major Indian ports using the dual reciprocity boundary element technique," *Ocean Eng.*, vol. 341, p. 122524, 2025. doi: https://doi.org/10.1016/j.oceaneng.2025.122524.

[20] D. Dehghan-Souraki et al., "Three-dimensional finite element modeling of thermal stratification in the Riba-Roja Reservoir confluence: A fluid–thermal multiphysics approach," Water, vol. 17, no. 5, p. 674, 2025. doi: https://doi.org/10.3390/w17050674.